The CVB Experiment Constrained Bubble Nucleation In Microgravity

CONFERENCE PAPER · OCTOBER 2011

READS
20

9 AUTHORS, INCLUDING:

J.L. Plawsky
Rensselaer Polytechnic Institute
199 PUBLICATIONS **1,935** CITATIONS
SEE PROFILE

P. C. Wayner
Rensselaer Polytechnic Institute
146 PUBLICATIONS **2,620** CITATIONS
SEE PROFILE

John Eustace
ZIN Technologies, Inc.
17 PUBLICATIONS **21** CITATIONS
SEE PROFILE

Louis Chestney
Zin Technologies
9 PUBLICATIONS **18** CITATIONS
SEE PROFILE

Spreading, Evaporation, and Contact Line Dynamics of Surfactant-Laden Microdrops

Shripad J. Gokhale,[†,‡] Joel L. Plawsky,*[,†] and Peter C. Wayner, Jr.*[,†]

The Isermann Department of Chemical and Biological Engineering, Rensselaer Polytechnic Institute, Troy, New York 12180

Received March 7, 2005. In Final Form: May 11, 2005

An optical technique based on the reflectivity measurements of a thin film was used to experimentally study the spreading, evaporation, contact line motion, and thin film characteristics of drops consisting of a water−surfactant (polyalkyleneoxide-modified heptamethyltrisiloxane, called superspreader) solution on a fused silica surface. On the basis of the experimental observations, we concluded that the surfactant adsorbs primarily at the solid−liquid and liquid−vapor interfaces near the contact line region. At equilibrium, the completely wetting corner meniscus was associated with a flat adsorbed film having a thickness of ∼31 nm. The calculated Hamaker constant, $A = -4.47 \times 10^{-20}$ J, shows that this thin film was stable under equilibrium conditions. During a subsequent evaporation/condensation phase-change process, the thin film of the surfactant solution was unstable, and it broke into microdrops having a finite contact angle. The thickness of the adsorbed film associated with the drops was lower than that of the equilibrium meniscus. The drop profiles were experimentally measured and analyzed during the phase-change process as the contact line advanced and receded. The apparent contact angle, the maximum concave curvature near the contact line region, and the convex curvature of the drop increased as the drop grew during condensation, whereas these quantities decreased during evaporation. The position of the maximum concave curvature of the drop moved toward the center of the drop during condensation, whereas it moved away from the center during evaporation. The contact line velocity was correlated to the observed experimental results and was compared with the results of the drops of a pure alcohol. The experimentally obtained thickness profiles, contact angle profiles, and curvature profiles of the drops explain how the surfactant adsorption affects the contact line motion. We found that there was an abrupt change in the velocity of the contact line when the adsorbed film of the surfactant solution was just hydrated or desiccated during the phase-change processes. This result shows the effect of vesicles and aggregates of the surfactant on the shape evolution of the drops. For these surfactant-laden water drops, we found that the apparent contact angle increased during condensation and decreased during evaporation. However, for the drop of a pure liquid (*n*-butanol and 2-propanol) the apparent contact angle remained constant at a constant velocity during condensation and evaporation. The contact line was pinned during the evaporation and spreading of the surfactant-laden water drops, but it was not pinned for a drop of a pure alcohol (self-similar shape evolution).

I. Introduction

The phenomenon of spreading and evaporation of droplets is important in many applications such as coating (photographic films, automobile exteriors, photoresist deposition), surface cleaning, printing, spraying, dropwise condensation, and so forth. The presence of surfactants alters the behavior of drops on a solid surface, and surfactants are used to enhance the ability of a liquid to wet a solid surface. Surfactants can reduce the surface tension of liquids, so they are used as emulsifiers and dispersants. They are also used to increase the coating effectiveness of liquids sprayed onto various surfaces, especially biological surfaces.

One particular class of surfactants that has received much attention in this regard is the trisiloxane surfactant.[1−5] We studied experimentally the stability of a thin adsorbed film of a solution of trisiloxane surfactant in deionized (DI) water under equilibrium and nonequilibrium conditions. We were particularly interested in the effect of phase changes on the drop as it spreads because of condensation or contracts because of evaporation. The surfactant that we used was a polyalkyleneoxide-modified heptamethyltrisiloxane called Silwet-L77. The chemical structure of the surfactant[1] is shown in Figure 1. The surfactant molecule has a compact hydrophobic group and a long, hydrophilic polyether tail. Because of this particular structure, the surfactant molecule adsorbs at the solid−liquid and liquid−vapor interfaces. The addition of a small amount (0.01%) of this surfactant reduces the surface tension of water from 72 to about 21 mJ/m^2. In the solution, the surfactant molecules form aggregates and vesicles when present in a concentration above the critical aggregate concentration of 0.01%.[1−5] Because of the mutual repulsion of the vesicles, a thin film of the surfactant solution remains stable under isothermal conditions.

The trisiloxane surfactants are recognized as effective wetting agents for water-based herbicide sprays.[6] Plant leaves are waxy, and thus their surfaces are hydrophobic. Hence, they are difficult to wet with water-based sprays, so herbicides are difficult to apply uniformly. The ability

* Corresponding authors. E-mail: plawsky@rpi.edu, Phone: 518-276-6049, Fax: 518-276-4030. E-mail: wayner@rpi.edu, Phone: 518-276-6199, Fax: 518-276-4030.

† Rensselaer Polytechnic Institute.

‡ Current Affiliation: Intel Corporation, Chandler, Arizona.

(1) Zhu, S.; Miller, W. G.; Scriven, L. E.; Davis, H. T. *Colloids Surf.* **1994**, *90*, 63.

(2) Ananthapadmanabhan, K. P.; Goddard, E. D.; Chandar, P. *Colloids Surf.* **1990**, *44*, 281.

(3) Wagner, R.; Wu, Y.; Czichocki, G.; Berlepsch, H. V.; Rexin, F.; Perepelittchenko, L. *Appl. Organomet. Chem.* **1999**, *13*, 201.

(4) Churaev, N. V.; Esipova, N. E.; Hill, R. M.; Sobolev, V. D.; Starov, V. M.; Zorin, Z. M. *Langmuir* **2001**, *17*, 1338.

(5) Nikolov, A. D.; Wasan, D. T.; Chengara, A.; Koczo, K.; Policello, G. A.; Kolossvary, I. *Adv. Colloid Interface Sci.* **2002**, *96*, 325.

(6) Knoche, M.; Tamura, H.; Bukovac, M. J. *J. Agric. Food Chem.* **1991**, *39*, 202.

10.1021/la050603u CCC: $30.25
Published on Web 08/02/2005

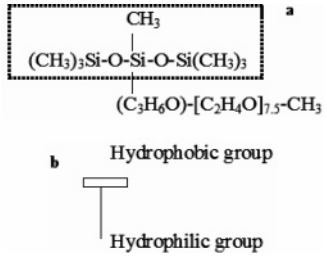

Figure 1. (a, b) Chemical structure of polyalkyleneoxide-modified heptamethyltrisiloxane (Silwet-L77).

of trisiloxane surfactants to promote the spreading of water on various hydrophobic surfaces is called superspreading, and because of this ability, they enable water-based spray solutions to effectively wet and protect the entire surface of plant leaves. These surfactants are also used to improve the stability of water-based paint films on hydrophobic soil surfaces.

The unique superspreading property of trisiloxane surfactants has been explained in the literature[1−6] on the basis of four factors: (a) the configuration and adsorption of trisiloxane molecules at the interfaces, (b) the formation of vesicle-type aggregates in the solution, (c) the ability to lower the liquid−vapor surface tension to very low values, and (d) Marangoni effects. Zhu et al.[1] found that a dispersed surfactant-rich phase is needed for superspreading and that the initial rate of spreading increases with decreasing size of the particles of the dispersed phase. They also concluded that the presence of water vapor is necessary for superspreading. Ananthapadmanabhan et al.[2] studied the solution, interfacial, and wetting properties of these surfactants using surface tension, adsorption, fluorescence, and fluorescence decay techniques. They attributed the special wetting properties of the trisiloxane surfactant to the structure of its adsorbed molecules. Wagner et al.[3] showed that the spreading and phase behavior of the trisiloxane surfactant are closely related. They found that the highest initial spreading rate occurs for solutions in the two-phase state above the single-phase liquid−liquid coexistence curve. Churaev et al.[4] investigated spreading and film climbing of trisiloxane surfactant solutions by including the concept of a disjoining pressure isotherm in the Navier−Stokes equations. Nikolov et al.[5] suggested that the spreading of trisiloxane surfactants is controlled by a surface tension gradient along the spreading front and by the molecular configuration at the air−water interface. All of these studies on trisiloxane surfactants and their ability to superspread address spreading under isothermal conditions. To the best of our knowledge, the effect of phase changes on spreading and drop formation containing trisiloxane surfactants has not been addressed in the literature. In this article, we present an experimental investigation of a static meniscus and the associated adsorbed film of the trisiloxane surfactant on a fused silica surface under isothermal conditions. We also investigated experimentally how the thin adsorbed film of the surfactant solution breaks into microdrops. We studied the contact line motion and shape evolution of the microdrops during evaporation and condensation in a saturated environment using reflectivity measurements. The contact line velocity was defined on the basis of the position of the zeroth dark fringe in the reflectivity profiles of drops (film thickness = 0.1 μm) as a reference. These studies help us to understand the effect of the trisiloxane surfactant on the physics of contact line motion and the shape evolution of droplets during phase-change processes.

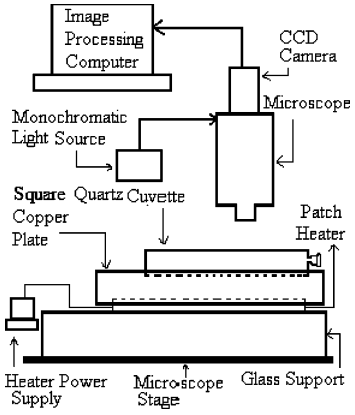

Figure 2. Schematic drawing of the experimental setup.

In the experimental system (Figure 2),[7−10] the surfactant solution formed menisci in the corners of a fused silica cuvette with a square cross section and an adjacent thin adsorbed film on the surface under isothermal equilibrium conditions. A change in vapor pressure due to a phase change caused the adsorbed film to break up into microdrops, which grew on the fused silica surface during condensation and contracted during evaporation. In a 1957 seminal paper, Derjaguin and Zorin[11] demonstrated that a thin, adsorbed, flat film of *n*-propyl alcohol became unstable at the saturation point at a film thickness of approximately 5.5 nm. Above this thickness, they viewed "microdewdrops" on an adsorbed layer. Therefore, the adsorption isotherm near the saturation point is very complex for a fluid.[11] The important process of dropwise condensation occurs in this region of the adsorption isotherm. The macroscopic observations of the condensing and evaporating drops and the associated adsorbed thin film reported herein are consistent with the observations of Derjaguin and Zorin.[11]

We measured the microscopic details of the defining characteristics (thickness profile and surrounding adsorbed film thickness) of the condensing and evaporating drops and of the isothermal meniscus formed on a fused silica surface. We studied the growth and evaporation of these microdewdrops using high-resolution microinterferometry. There is a lack of experimental data concerning these details. A technique based on the analysis of the reflectivity profiles[9,10,12] was used to obtain the thickness, slope, and curvature profiles of these drops, including the profiles in the contact line region. The results from the isothermal studies explain the stability of the adsorbed film of the surfactant solution on the fused silica surface on the basis of the concept of the minimization of interfacial free energy. The experimental results also indicate that the slope angle, curvature, and curvature gradient govern the pressure fields in the drops. The experimentally obtained contact line velocity during spreading and evaporation, the slope angle (a measure of the apparent contact angle of the drop), and the curvature profiles

(7) Gokhale, S. J.; Plawsky, J. L.; Wayner, P. C., Jr. *J. Colloid Interface Sci.* **2003**, *259*, 354.
(8) Gokhale, S. J.; Plawsky, J. L.; Wayner, P. C., Jr. *Adv. Colloid Interface Sci.* **2003**, *104*, 175.
(9) Gokhale, S. J.; Plawsky, J. L.; Wayner, P. C., Jr.; DasGupta, S. *Phys. Fluids* **2004**, *16*, 1942.
(10) Gokhale, S. J.; DasGupta, S.; Plawsky, J. L.; Wayner, P. C., Jr. *Phys. Rev. E* **2004**, *70*, 051610.
(11) Derjaguin, B. V.; Zorin, Z. M. *Proc. Int. Congr. Surf. Act.* **1957**, *2*, 145.
(12) DasGupta, S.; Plawsky, J. L.; Wayner, P. C., Jr. *AIChE J.* **1995**, *41*, 2140.

explain how the adsorption of the surfactant at the interfaces affects the evolution of drops.

II. Materials and Methods

A. Surfactant Solution Preparation and Fused Silica Cell Pretreatment. A schematic diagram of the experimental setup is shown in Figure 2. The experimental cell[7−10] consisted of a UV-grade fused silica cuvette with inside dimensions of 3 mm × 3 mm, outside dimensions of 5.5 mm × 5.5 mm, and length 43 mm. Prior to the experiments, the cuvette was heat treated in an oven at 150 °C for 45 min to remove any adsorbed impurities. It was then partially filled with the working liquid (∼3 mL) inside a controlled environment of nitrogen. The cuvette was closed with a Teflon stopper. Therefore, the "vapor" space was composed of vapor, nitrogen, and a small amount of air. The liquid used here was a 1% (by weight) solution of Silwet L-77 surfactant (polyalkyleneoxide-modified heptamethyltrisiloxane, obtained from Crompton Corporation) in DI water. This concentration is much higher than the critical aggregate concentration of this surfactant. The solution was sonicated for about 15 min before filling the cuvette to form a uniform dispersion. The surface tension of the solution was measured using a Fisher surface tensiomat and was found to be 21 mJ/m^2. The surface tension of pure water was measured to be 72 mJ/m^2 under the same conditions. The entire setup was slightly inclined.

B. Experimental Setup and Procedure. The fused silica cell was mounted axially on a copper plate. An insulated flexible heater (from Omega Engineering, Inc.) was attached to the bottom of the copper plate. A thermoelectric heater was attached to the top of the cuvette. The experimental system consisting of the fused silica cuvette, partially filled with the surfactant solution, was allowed to equilibrate for about 1 day. The surfactant formed menisci in the corners of the cuvette and a thin adsorbed film on the surface of the cuvette under isothermal conditions. A continuous liquid path connected all of the menisci.

To study the condensation of the droplets, a small amount of power was applied to the heater at the bottom of the copper plate. Vapors of the surfactant solution formed inside the fused silica cell condensed on the upper surface inside the cell because it was at a slightly lower temperature. Because the surfactant solution partially wet the fused silica surface above a critical thickness, we observed dropwise condensation of the surfactant and mutual interaction of the drops on the top surface inside the cuvette. To study the evaporation of the droplets, a small amount of power was applied to the thermoelectric heater attached to the top of the cuvette. The entire setup was mounted on a microscope stage as shown in Figure 2. The spreading of the drop resulted from the combined effects of liquid flow toward the contact line region due to the pressure gradient within the drop and the phase-change process occurring at the liquid−vapor interface of the drop.[7,10]

An imaging technique[4,9,12−14] based on the measured reflectivity of the liquid film at each pixel location along the entire drop profile relative to that of the calibrated bare surface (which corresponds to an adsorbed film thickness equal to zero) was used to measure the drop shape. Monochromatic light ($\lambda = 543.5$ nm) from a Hg arc was used as the light source. Naturally occurring interference fringes result from the reflection of light at the liquid−vapor and the solid−liquid interfaces as demonstrated by the optical micrographs presented in Figure 3. A CCD camera (with a maximum frame rate of 30 frames/s) was used to capture the images of the reflectivity pattern of the drops. The captured images were digitized into 640 × 480 pixels and assigned 1 of 256 possible gray values representing intensity from 0 (black) to 255 (white). We thereby measured how the liquid−vapor interfacial profile changes from convex in the thicker portion of the drop to concave in the thinner portion of the drop. Because of the difference in reflectivity, the experimental technique also demonstrated the presence of a thin, flat adsorbed film associated with the condensing or evaporating drops.

Imaging techniques giving fewer details have been used in the past to observe interfacial phenomena in various systems. For example, Wiegand[13,14] studied the wetting properties of micropatterned surfaces using this technique but called it reflection contrast interferometry. Blake[15] used double-wavelength interferometry to investigate equilibrium wetting films of alkanes on α-alumina. Wayner and co-workers[7,8,12,16−22] used ellipsometry and interferometry techniques to study the liquid−vapor interfacial phenomena during phase-change processes in both wetting and nonwetting systems. Chen and Wada[23] used laser interferometry to investigate microlayer spreading phenomena. Using our experimental technique, we were able to obtain additional details of the shape profiles.

C. Data Analysis Technique. The image analysis technique has been described in detail in previous publications.[9,10] Only a brief description is given here. From each image of a drop, a plot of the pixel gray value (G) versus pixel position (x) was extracted. A computer program scanned the reflectivity pattern and calculated a relative gray value at each pixel position using eq 1

$$\bar{G}(x) = \frac{G(x) - G_{\min}(x)}{G_{\max}(x) - G_{\min}(x)} \tag{1}$$

where $G_{\min}(x)$ and $G_{\max}(x)$ are the interpolated envelopes to the various-order minima and maxima (constructive and destructive fringes). Using the measured gray value of the bare surface of the cuvette (corresponding to zero film thickness) for calibration, the thickness (δ) at each pixel location was obtained from the relative gray value (RL) at that pixel location[9,10] using eqs 2−4

$$RL(x) = \bar{G}(x)[RL_{\max} - RL_{\min}] + RL_{\min} \tag{2}$$

$$RL = \frac{\alpha + \beta \cos 2\theta_l}{\kappa + \beta \cos 2\theta_l} \tag{3}$$

where

$$\theta_l = \frac{2\pi n_l \delta}{\lambda} \qquad \alpha = r_1^{\,2} + r_2^{\,2} \qquad \beta = 2r_1 r_2$$

$$\kappa = 1 + r_1^{\,2} r_2^{\,2} \qquad r_1 = \frac{n_l - n_v}{n_l + n_v} \qquad r_2 = \frac{n_s - n_l}{n_s + n_l} \tag{4}$$

Here, n_v, n_s, n_l are the refractive indices of vapor, solid, and liquid phases, respectively, and λ is the wavelength of light.

The slope ($d\delta/dx$) of the thickness profile (local slope angle) and the curvature (K) were obtained at pixel number p by fitting a second-order polynomial (coefficient of regression greater than 0.99) to the thickness at pixel numbers $p - 1$, p, and $p + 1$. The diameter of a pixel was 0.177 μm. The curvature was calculated using eq 5.

$$K = \frac{\dfrac{d^2\delta}{dx^2}}{\left[1 + \left(\dfrac{d\delta}{dx}\right)^2\right]^{3/2}} + \frac{\dfrac{d\delta}{dx}}{x\left[1 + \left(\dfrac{d\delta}{dx}\right)^2\right]^{1/2}} \tag{5}$$

Thus, the technique successfully measures the film thickness and evaluates the slope and curvature at every pixel position. This technique captures the variations of these quantities as a function of position. All of the data from the isothermal meniscus

(13) Wiegand, G.; Jaworek, T.; Wegner, G.; Sackmann, E. *J. Colloid Interface Sci.* **1997**, *196*, 299.
(14) Wiegand, G.; Neumaier, K. R.; Sackmann, E. *Appl. Opt.* **1998**, *37*, 6892.
(15) Blake, T. D. *J. Chem. Soc., Faraday Trans. 1* **1975**, *71*, 192.
(16) Renk, F.; Wayner, P. C., Jr.; Homsy, G. M. *J. Colloid Interface Sci.* **1978**, *67*, 408.
(17) Renk, F.; Wayner, P. C., Jr. *J. Heat Transfer* **1979**, *101*, 55.
(18) Truong, J. G.; Wayner, P. C., Jr. *J. Chem. Phys.* **1987**, *87*, 4180.
(19) Liu, A. H.; Wayner, P. C., Jr.; Plawsky, J. L. *Phys. Fluids* **1994**, *6*, 1963.
(20) Wang, Y.-X.; Plawsky, J. L.; Wayner, P. C., Jr. *Microscale Thermophys. Eng.* **2001**, *5*, 55.
(21) Zheng, L.; Wang, Y.-X.; Plawsky, J. L.; Wayner, P. C., Jr. *Langmuir* **2002**, *18*, 5170.
(22) Zheng, L.; Wang, Y.-X.; Plawsky, J. L.; Wayner, P. C., Jr. *Int. J. Heat Mass Transfer* **2002**, *45*, 2021.
(23) Chen, J. D.; Wada, N. *J. Colloid Interface Sci.* **1992**, *148*, 207.

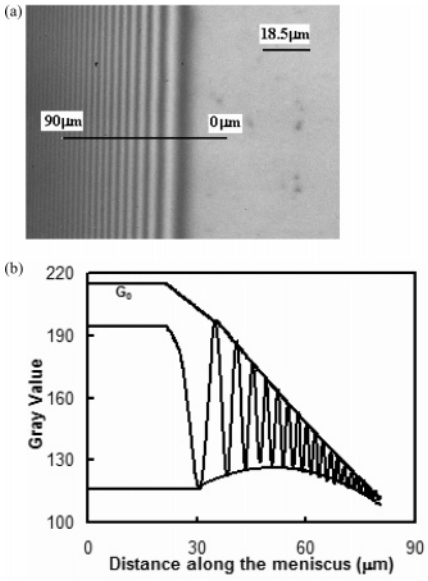

Figure 3. (a) Optical micrograph of the corner meniscus of the surfactant solution under isothermal equilibrium conditions. (b) Reflectivity profile of the meniscus of the surfactant solution under isothermal equilibrium conditions.

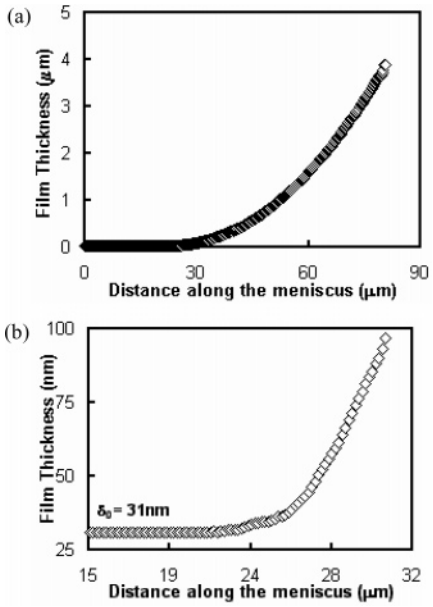

Figure 4. (a) Thickness profile of the meniscus of the surfactant solution under isothermal equilibrium conditions. (b) Thickness profile of the meniscus of the surfactant solution near the adsorbed thin film region under isothermal equilibrium conditions.

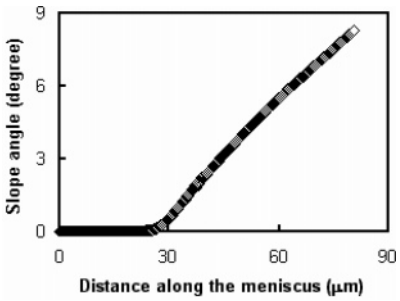

Figure 5. Slope-angle profile of the meniscus of the surfactant solution under isothermal equilibrium conditions.

and condensing and evaporating drop images were analyzed using this technique. Validation of the experimental technique is discussed in a recent publication.[10]

The experimental technique presented here is limited to the measurement of small contact angles (<13°). This also limits the measurement of the maximum film thickness to about 4 μm. To obtain quality, high-contrast reflectivity images, the difference between the refractive indices of the solid and the liquid should be as high as possible.[12] As discussed in ref 9, the error associated with the film-thickness measurement in the transition and capillary regions of the film was estimated to be $\pm$0.01 μm.

III. Results and Discussion

A. Isothermal (Equilibrium) Studies. It is known in the literature[1−5] that trisiloxane surfactants spread completely on a fused silica surface and form a stable adsorbed thin film at equilibrium. Experimentally, we characterized the thickness of the thin adsorbed film and the strength of the intermolecular forces at conditions as close to equilibrium at 25 °C as we could realistically attain.

Initially, the experimental system consisting of the fused silica cuvette partially filled with the surfactant solution was allowed to equilibrate for about 1 day. The surfactant formed menisci in the corners of the cuvette and a thin adsorbed film on the surface of the cuvette. Figure 3 shows the experimentally obtained optical micrograph and the corresponding reflectivity profile of the surfactant meniscus under isothermal conditions. The thickness profile, obtained from the reflectivity scan, is shown in Figure 4. We see that the meniscus was concave and had a positive curvature in the thicker region. There was a thin adsorbed film (on the surface of the cuvette) in equilibrium with the corner meniscus. A positive curvature of the liquid−vapor interface (of the meniscus) represents a decrease in the vapor pressure of the liquid, P_{vlv}, compared to that of a bulk flat film and a pressure jump at the liquid−vapor interface between the pressure in the vapor−air space, P_{va}, and the liquid, P_l, as represented by the augmented Young−Laplace equation (eq 6) and the chemical potential gradient at the liquid−vapor interface.[15−17,24−27]

$$P_{va} - P_l = K\sigma - \frac{A}{6\pi\delta_0^3} \qquad (6)$$

Here, A is the Hamaker constant, which represents the system-specific parameter proportional to the van der Waals interaction. σ is the surface tension, and P_{va} and P_l represent the pressures in the vapor−air and the liquid phases, respectively. δ_0 is the experimentally obtained thickness of the adsorbed film at equilibrium (31 nm). K is the curvature of the meniscus. Thus, the vapor space inside the cuvette was saturated at isothermal conditions.

The corresponding slope angle and the curvature profiles (calculated using eq 5) are shown in Figures 5 and 6, respectively. In the limit for a corner meniscus, the second term in eq 5 becomes zero. Hence, we can still use eq 5 for the corner meniscus (as is done for Figure 6); however, the second term in eq 5 is negligible for the data shown in Figure 6. We see that the apparent contact angle (defined here as the slope angle at a film thickness of 0.1 μm) was very small (1°) and the slope was zero in the adsorbed film region. Thus, the surfactant solution completely wets the fused silica surface and forms an adsorbed film. From Figure 6, we see that the curvature was zero in the adsorbed thin film region. The curvature of the corner meniscus was positive and increased as the

(24) Derjaguin, B. V. *Acta Physicochim.* **1940**, 12, 181.
(25) Derjaguin, B. V.; Kusakov, M. *Acta Physicochim.* **1939**, *10*, 153.
(26) Read, A. D.; Kitchener, J. A. *Soc. Chem. Ind. Monogr.* **1967**, 300.
(27) Potash, M.; Wayner, P. C., Jr. *Int. J. Heat Mass Transfer* **1972**, *15*, 1851.

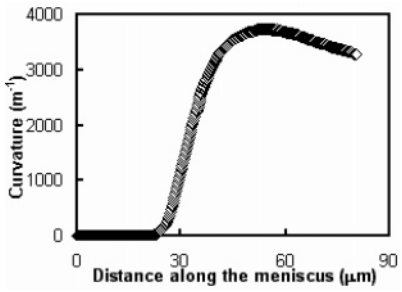

Figure 6. Curvature profile of the meniscus of the surfactant solution under isothermal equilibrium conditions.

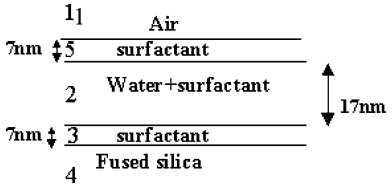

Figure 7. Schematic drawing of the adsorbed film of the surfactant solution on the solid surface at equilibrium.

film thickness increased along the meniscus. In the thicker region, it became constant. The slight change in the curvature in Figure 6 for the thicker region represents the effect of the other wall. The constant value of the curvature for the corner meniscus of the surfactant solution was about 3400 m^{-1}. The experimental data of the film thickness and the curvature of the meniscus at equilibrium can be used to study the stability of the thin adsorbed film using the concept of minimization of the interfacial energy. This is described in the following discussion. We assume that, for the range of the experimental film thickness values reported here only van der Waals forces contribute to the interfacial free energy.[28] Other interactions, such as structural forces, are neglected.

Using the augmented Young−Laplace equation (eq 6), the experimental values of the adsorbed film thickness, and the curvature of the corner meniscus in the thicker region (3400 m^{-1}), the experimental value of the Hamaker constant (A) was calculated to be -4.4×10^{-20} J.

The Hamaker constant was theoretically estimated on the basis of a multilayer film model[29] (eq 7), sketched schematically with this subscript code in Figure 7. The surfactant phase was assumed to form a separate layer near the solid surface and near the air phase, the thickness of which was calculated on the basis of the chain length of the surfactant:

$$\frac{A_{\text{theoretical}}}{{l_{523}}^2} = -\frac{A_{22} - A_{523}}{{l_2}^2} + \frac{A_{24} - A_{523}}{{l_{523}}^2} \qquad (7)$$

The individual Hamaker constants in eq 7 were calculated on the basis of the dielectric constants and the refractive indices of the different phases involved.[28] The values of the terms in eq 7 were $A_{22} = -3.73 \times 10^{-20}$ J, $A_{523} = -2.93 \times 10^{-22}$ J, $A_{24} = -1.49 \times 10^{-20}$ J, $l_{523} = 24$ nm, and $l_2 = 17$ nm. On the basis of these values, the theoretical value of the Hamaker constant was estimated to be -7.2×10^{-20} J. This value is in good agreement with the experimental value and indicates that the disjoining pressure model based on eq 6 was applicable at this thickness.

A negative value of the Hamaker constant represents a positive disjoining pressure (Π). This implies that the free energy of the film (ΔG) decreases[28,30−32] as the film thickness increases (eq 8):

$$\Pi = -\frac{\partial \Delta G}{\partial \delta} \qquad (8)$$

Hence, the ~31 nm adsorbed film of the surfactant solution was stable under isothermal conditions. The presence of an adsorbed film of surfactant or surfactant solution was also demonstrated in the experiments of dropwise condensation and evaporation of the surfactant. However, the thickness of the adsorbed film between the droplets was significantly lower during these phase-change processes compared to the equilibrium condition. This will be explained in the next section.

B. Drop Formation during Evaporation and Condensation. To study the dropwise condensation of the surfactant solution on the fused silica surface, a small amount of power was applied to the heater at the bottom of the cuvette. The vapors of the surfactant solution formed inside the cell condensed on the upper surface inside the cell because it was at a slightly lower temperature. To study the evaporation of the droplets, a small amount of power was applied to the thermoelectric heater at the top of the cuvette. Because the observed formation of the drops is a nonequilibrium process, we used a chemical potential model (eqs 9 and 10) for mass transfer to describe the formation of drops that includes an isothermal Kelvin effect (disjoining pressure, capillarity, and gravity) and an isobaric Clapeyron effect.[7,8,12,16,27,33]

$$\Delta\mu_g = -(K\sigma + \Pi - \rho_l g x) + \frac{\rho_l \Delta h_m}{\bar{T}}(T_{lv} - T_v) \qquad (9)$$

$$\Delta\mu_g = \rho_{lm} R_g T_{lv} \ln \frac{P_{vlv}}{P_v} \qquad (10)$$

Here, $\Delta\mu_g$ is the change in chemical potential per unit volume (J/m^3), the vapor pressure in the bulk vapor−air space at x is P_v, and P_{vlv} is the vapor pressure at the liquid−vapor interface at x. The difference between these two vapor pressures can be used to obtain the interfacial mass flux. At equilibrium, these two vapor pressures are equal. The interfacial vapor pressure is affected by the capillary pressure ($K\sigma$), the disjoining pressure (Π), the hydrostatic head ($\rho g x$), and the temperature. ρ_{lm} is the liquid molar density (moles/m^3), whereas ρ_l is the liquid density (kg/m^3). The interfacial temperature jump is $\Delta T = T_{lv} - T_v$. The product of the density, ρ_l, and the latent heat of vaporization, Δh_m, is the volumetric heat of vaporization at the average phase-change temperature, $\bar{T}$. Equation 9 connects the thin film superheat with the isothermal thin film free energy per unit volume. The disjoining pressure describes the interfacial chemistry of adhesion versus cohesion. A positive disjoining pressure and/or capillary pressure (concave toward the vapor) leads to a reduction in the interfacial vapor pressure (Kelvin effect), which can be modified by a change in the interfacial temperature (Clapeyron effect).

According to eqs 9 and 10, $\Delta\mu > 0$ corresponds to evaporation, and $\Delta\mu < 0$ corresponds to condensation. At

(28) Israelachvili, J. N. *Intermolecular and Surface Forces*; Academic Press: London, 1992.
(29) Müller, M.; MacDowell, L. G.; Müller-Buschbaum, P.; Wunnike, O.; Stamm, M. *J. Chem. Phys.* **2001**, *115*, 9960.
(30) Sharma, A. *Langmuir* **1993**, *9*, 861.
(31) Sharma, A. *J. Colloid Interface Sci.* **1998**, *199*, 212.
(32) Correa, R.; Saramago, B. *J. Colloid Interface Sci.* **2004**, *270*, 426.
(33) Wayner, P. C., Jr. *Colloids Surf.* **1991**, *52*, 71.

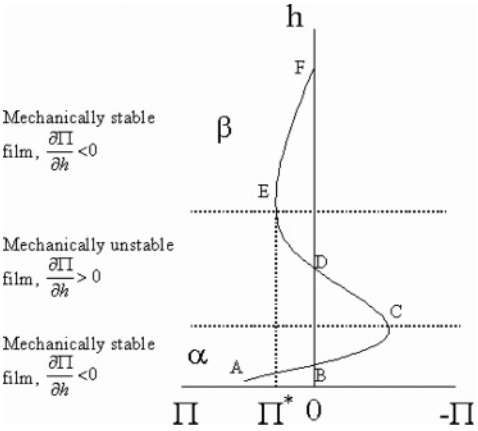

Figure 8. Schematic of the disjoining pressure isotherm (Kelvin part neglecting gravity, $-\Delta\mu = \Pi$) of the surfactant solution.[4]

isothermal equilibrium, this gives eq 11 for an extended meniscus on a flat surface:

$$K\sigma + \Pi = \rho_l g x = P_{va} - P_l \qquad (11)$$

In the isothermal limit without the gravitational term, this leads to the model used by Churaev et al.[4] to describe the formation of the drops using the schematic disjoining pressure isotherm of a trisiloxane surfactant solution (Figure 8, in which the effect of gravity is neglected). On the basis of this isotherm, a film of the surfactant solution is mechanically unstable in a film thickness range of $h_C < h < h_E$. In our case, the initial equilibrium flat film thickness of 31 nm on the upper surface of the cuvette presented in Figure 4b is a β film represented by $\rho_l g x = \Pi$ and $K\sigma = 0$ in eq 11. The region of the mechanically stable β film corresponds to film thickness values higher than that represented by point E ($h = h^*$) in Figure 8. Upon evaporation, with a decrease in film thickness, the film becomes unstable at $h = h^*$ and forms droplets with a thinner α film ($h < h_B$) between them. Because the thinner film of the surfactant solution partially wets the fused silica surface at saturation, we could subsequently observe dropwise condensation of the solution on the top surface inside the cuvette. The menisci in the corners of the cuvette were due to condensation and the capillary flow of the liquid from/to the pool at the bottom.

Because of heating and cooling, extremely small temperature differences[7] estimated to be less than 10^{-4} K, which cannot be detected experimentally, occurred at the liquid−vapor interface during the phase-change experiments. However, the pressure field, which can be used to calculate internal flow patterns numerically, can be obtained from the measured profiles and used to help understand the transition process. In the course of evaporative thinning of the films ($\beta \rightarrow \alpha$ transition), droplets are formed in the region shown by a negative value of the disjoining pressure (region between points B and D in Figure 8). Thus, after the $\beta \rightarrow \alpha$ phase transition occurring during evaporation, thin adsorbed α films are formed around the droplets because of vapor adsorption.[4] This analysis is consistent with the adsorption isotherm of a partially wetting polar liquid discussed by Sharma.[34] In ref 34, it was postulated that branch AB is realized upon increasing the vapor pressure but decreasing the vapor pressure traces branch FE, followed by a downward jump at point E to branch AB.

(34) Sharma, A. *Langmuir* **1998**, *14*, 4915.

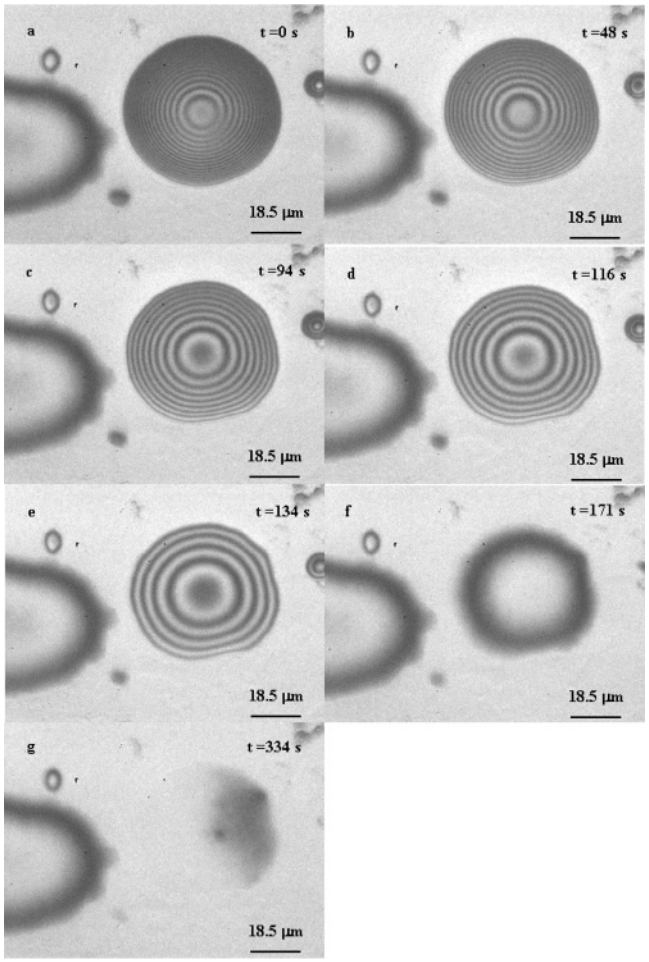

Figure 9. (a−g) Optical micrographs of the evaporating drop of the surfactant solution on the fused silica surface as a function of time.

C. Evaporating Drop. The experimentally obtained micrographs of the evaporating drops of the surfactant solution are shown in Figure 9. We note that the reflectivity images were obtained every 1 s, but we present only representative time instants in Figure 9. The region to the left of the drop is very complicated because it represents the edge of the corner meniscus with a varying profile in the x and y directions. The left-hand portion of Figure 9 is a picture of the start of this region. The sequence of the experimentally obtained optical micrographs of the corner meniscus during the evaporation cycle is shown in Figure 10. It shows the breakup of the adsorbed film on the surface (Figure 10a) due to evaporation. We note that the relative time instances shown in Figure 10a−d do not correspond to the same time instances as shown in Figure 9a−g.

For each of these drops, the film thickness profiles are shown in Figure 11. The experimental data shows the presence of a thin uniform adsorbed film associated with the evaporating drop. The thickness of the adsorbed film was 6 nm and remained constant during evaporation. We hypothesize that this film thickness corresponds to the region just above point B in Figure 8. On the basis of the estimates of the hydrophilic chain length of the surfactant molecules, the thickness of the vesicle wall is about 7 nm. This value is very close to the experimentally observed thickness of the adsorbed film. At the end of the evaporation of the drop (Figure 9g), a thin film of the surfactant solution remained adsorbed at the location of the drop. As demonstrated below, the film thickness profile was concave

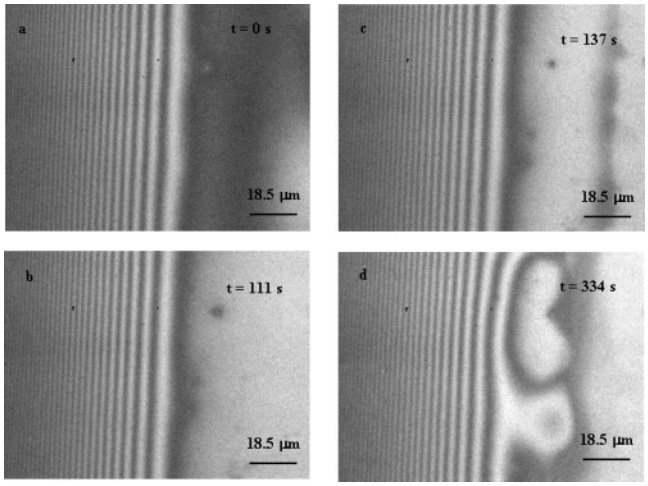

Figure 10. (a–d) Optical micrographs of the evaporating corner meniscus of the surfactant solution on the fused silica surface as a function of time

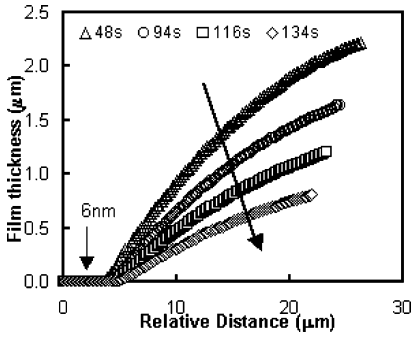

Figure 11. Film thickness profiles of the drop during evaporation as a function of time.

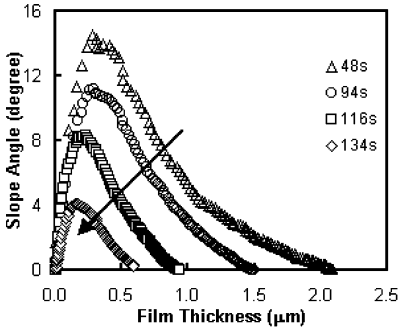

Figure 12. Slope-angle profiles of the drop during evaporation as a function of time.

near the contact line region (microscopic region) and convex in the thicker portion of the drop.

The slopes of the film thickness profiles ($d\delta/dx$) corresponding to Figure 11 are plotted in Figure 12 against the film thickness along the drop. In the adsorbed thin film region, the slope of the film thickness profile (and hence the real microscopic contact angle) was constant and zero. This result is in agreement with the modeling results of Anderson and Davis[35] and Hocking.[36] Hocking[36] used the condition of the initial slope of the thickness profile equal to zero to solve the evolution equation of an evaporating drop. From the minimization of the free energy, the microscopic contact angle at the contact line would always be zero (e.g., refs 37–39). The slope of the film-thickness

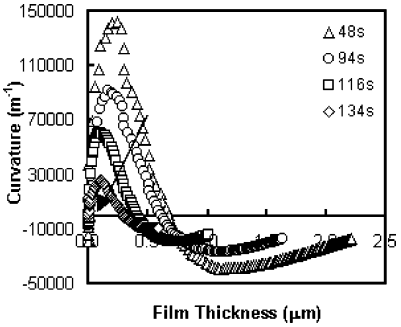

Figure 13. Curvature profiles of the drop during evaporation as a function of time.

profile then increased as the film thickness increased and passed through a maximum. The slope then decreased and became zero in the thicker portion of the drop. As demonstrated in previous models, an "apparent contact angle" is a function of the film thickness[15,27,35–40] and needs to be carefully defined. We defined the maximum angle in the slope-angle profile of the drop as the apparent contact angle of the drop. This represents a region near the contact line region where the profile of the drop changes from concave to convex. The apparent contact angle of the drop decreased during the evaporation of the drop. The position of the maximum in the slope angle occurred at smaller and smaller film thicknesses during evaporation. Thus, the drop shape changed in a non-self-similar manner during evaporation. This is explained later on the basis of the velocity of the contact line and is compared with the self-similar shape evolution of a pure fluid.

The curvature profiles calculated using the experimental data and eq 5 for the evaporating drop are shown in Figure 13. The curvature was zero in the adsorbed thin film region. In the contact line region, it was positive (concave thickness profile) and increased with an increase in the thickness. It passed through a maximum positive value at $\delta = \delta_{max}$, and in the thicker portion of the drop, the curvature was negative (convex thickness profile). Thus, the profile of the drop changed from a thin flat film ($K = 0$) to concave ($K > 0$) and then to a convex ($K < 0$). The magnitudes of both the maximum concave curvature and the convex curvature near the apex of the drop decreased during the evaporation of the drop. The position of the maximum (positive) curvature occurred at smaller and smaller film thicknesses as the drop evaporated, following the same trend as the interfacial slope.

D. Condensing Drop. Similar but opposite trends were obtained during the dropwise condensation experiments. At the end of the evaporation cycle ($t = 480$ s), the drop was made to condense by applying power to the heater attached to the bottom of the cuvette (Figure 2). Figure 14 shows the experimentally obtained micrographs of the condensing drop as a function of time. During condensation, the vapor initially condensed on the film of the surfactant (Figure 14a), which had remained adsorbed on the solid surface at the end of the evaporation cycle. We note that condensation occurred only where the original evaporating drop was present. Corresponding thickness, slope, and curvature profiles of the drop are plotted in Figures 15–17, respectively. During condensation, the thickness of the adsorbed film surrounding the

(35) Anderson, D. M.; Davis, S. H. *Phys. Fluids* **1995**, *7*, 248.
(36) Hocking, L. M. *Phys. Fluids* **1995**, *7*, 2950.
(37) Wayner, P. C., Jr. *J. Colloid Interface Sci.* **1980**, *77*, 495.
(38) Solomentsev, Y.; White, L. R. *J. Colloid Interface Sci.* **1999**, *218*, 122.
(39) Hirasaki, G. J. *Contact Angle, Wettability and Adhesion*; Mittal, K. L., Ed.; VSP: Amsterdam, 1993.
(40) Deryagin, B. V.; Starov, V. M.; Churaev, N. V. *Colloid J.* **1976**, *38*, 875.

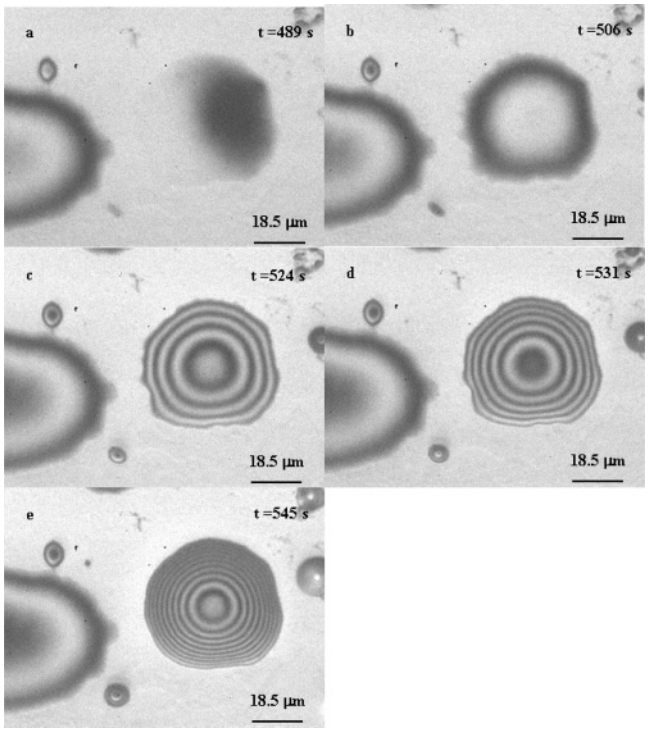

Figure 14. (a−e) Optical micrographs of the condensing drop of the surfactant solution on the fused silica surface as a function of time.

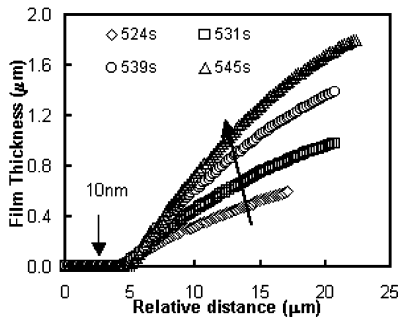

Figure 15. Film-thickness profiles of the drop during condensation as a function of time.

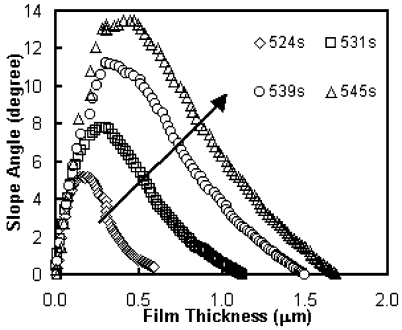

Figure 16. Slope-angle profiles of the drop during condensation as a function of time.

drop was higher (10 nm) than that during evaporation, and that thickness remains constant as the drop grows. This thickness corresponds to the region just above point D in Figure 8. We note that the thickness of the adsorbed film surrounding the drop (during the phase change) was lower than that observed for the meniscus under isothermal conditions (Figure 4). This is in agreement with the disjoining pressure isotherm presented in Figure 8, where

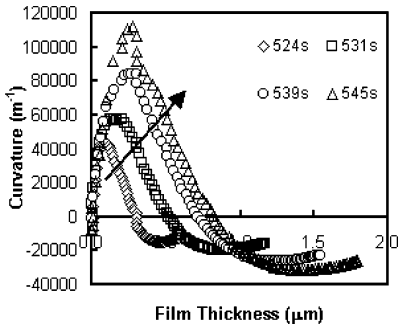

Figure 17. Curvature profiles of the drop during condensation as a function of time.

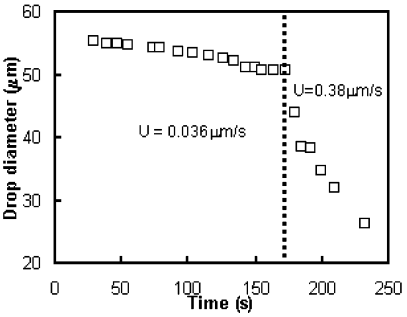

Figure 18. Drop diameter (based on the position of the zeroth-order dark fringe) as a function of time during evaporation. The dotted line corresponds to a relative time, $t = 170$ s.

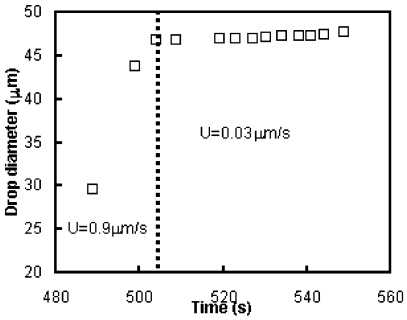

Figure 19. Drop diameter (based on the position of the zeroth-order dark fringe) as a function of time during condensation. The dotted line corresponds to a relative time, $t = 505$ s.

the α films surrounding the droplets are thinner than the metastable β films.

Figure 16 shows that the apparent contact angle of the drop increased during condensation. Figure 17 shows that the magnitudes of the maximum value of the curvature and the convex curvature near the apex of the drop increased as the drop grew during condensation. These results are exactly opposite to those observed during the evaporation of the drop. The positions of the maximum in the slope-angle profile and (positive value of) the curvature profile moved toward the center of the drop or toward higher and higher film thicknesses during condensation.

E. Contact Line Motion. We calculated the base diameter of the evaporating and condensing drops on the basis of the position of the zeroth order dark fringe ($\delta \approx$ 100 nm), which can be easily observed in the reflectivity images (Figures 10 and 14) as the reference. The evolution of the diameter of the evaporating and condensing drops as a function of time is plotted in Figures 18 and 19, respectively. We see that during the initial stage of evaporation (relative time, $t < 170$ s), when there was plenty of water in the drop, the rate of change of the drop diameter with respect to time (contact line velocity, U)

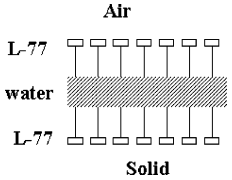

Figure 20. Schematic drawing of the surfactant molecule assembly at the critical time instant.

was very small (0.036 μm/s). The contact line was essentially pinned at the initial drop radius. However, for $t > 170$ s, the velocity was an order of magnitude higher (0.38 μm/s) because the last traces of readily evaporable water were removed. The actual contact line may still be pinned but was unobservable in our system. Similarly, during the initial stage of the condensation cycle (relative time, $t < 505$ s), the contact line velocity was relatively high (0.9 μm/s) because the drop became hydrated again. However, for $t > 505$ s, the velocity was an order of magnitude smaller (0.03 μm/s), and the contact line again appeared to be pinned at the initial radius of the drop ($t = 0$). We called the instant in time at which this sudden change in the kinetics of the contact line motion occurred a "critical time". We can calculate the critical mass of the drop at this instant, assuming that the drop formed a spherical cap on the surface.[7] The volume of this spherical cap (V_l) and the surface area of the liquid−vapor interface (A_{lv}) are given by the following relations:

$$V_l = \frac{\pi R^3}{3}(1 - \cos\theta)^2(2 + \cos\theta) \tag{12}$$

$$A_{lv} = 2\pi R^2(1 - \cos\theta) \tag{13}$$

Here, R is the radius of curvature of the drop, and θ is the apparent contact angle. We defined a characteristic length of the drop based on the liquid−vapor interfacial area and drop volume as

$$L_c = \frac{V_l}{A_{lv}} \tag{14}$$

On the basis of the experimental data, at the critical time instant ($t = 505$ s during condensation and $t = 170$ s during evaporation of the drop), the apparent contact angles of the evaporating and the condensing drop were 2.3 and 2.5°, respectively, and their base diameter, 47.5 mm, were also the same. The optical micrographs of the drops at these critical time instants showed that the maximum film thicknesses at the center were equal (0.2 μm, corresponding to the first bright fringe). Using these data, the critical volume of the drop at both critical times was calculated to be 4.1×10^{-7} μL. The density of the surfactant (1007 kg/m^3) is very close to that of water. Hence, the critical mass at which the sudden change in the contact line motion occurs during both evaporation (receding contact line) and condensation (advancing contact line) was 4.2×10^{-4} μg. Using eq 14, the characteristic length of the drop at this time instant was 0.23 μm. These calculations show that the critical point in the motion of the contact line is independent of the hysteresis of the contact line.

The faster kinetics of the contact line motion beyond the critical time can be explained on the basis of the typical adsorption of the trisiloxane surfactant at solid−liquid and liquid−vapor interfaces and the surfactant's ability to form aggregates in the solution.[1−5] Figure 20 shows a schematic of the surfactant molecule assembly at the critical time. The trisiloxane surfactant has a compact hydrophobic group and a long ether chain, and its concentration was above the critical aggregate concentration in the experiment. Hence, the surfactant molecules form a self-assembled structure in such a way that the hydrophobic headgroups are oriented away from the aqueous phase and toward the liquid−vapor and solid−liquid interfaces. The water phase is trapped within this self-assembled structure. At the critical time during evaporation, when the size of the drop (base diameter and maximum height at the center of the drop) is very small, the surfactant molecules try to achieve this self-assembled structure because thermodynamically it is the most stable structure for the trisiloxane molecules. Hence, the contact line motion of the drop became fast (as shown in Figures 18) for $t > 170$ s because evaporation was assisted by the self-assembly process. We hypothesized that the dehydrated self-assembled structure of the surfactant molecules on the surface during evaporation corresponds to the region near point B in Figure 8 because of the following reasoning. Because of temperature-induced evaporation, the flat film decreases in thickness from the initial isothermal value (near point F in Figure 8) toward h^*. At h^*, the film becomes mechanically unstable because of $\partial\Pi/\partial h > 0$, and the liquid flows away from the region where $h = h^*$. This leads to a film of thickness of $h < h_C$. The transition from h^* to h_C is due to both the fluid flow and evaporation. For $h < h_C$, evaporation would cause a decrease in the film thickness. However, $\partial\Pi/\partial h < 0$ would cause fluid flow toward the thin film. Therefore, the film thickness remains in the region $h_B < h < h_C$. We hypothesized that the film thickness is close to h_B. We note that the evaporation was slow. The same type of phenomenon occurred during condensation. Prior to actual condensation, evaporation had led to a self-assembled state at a relatively high temperature. Thus the surfactant aggregate had assembled in a state appropriate for this temperature. When condensation started, the temperature dropped and the aggregate reassembled in a configuration appropriate for a lower temperature. Hence, it rapidly hydrated until $t > 507$ s and thereupon grew slowly. We hypothesized that the recently hydrated self-assembled structure of the surfactant molecules on the surface during condensation corresponds to the region near point D in Figure 8 for the following reason. Because of temperature-induced condensation, the flat film increases in thickness from h_B (achieved at the end of the evaporation) toward h_C. For $h_C < h < h_D$, the flat film becomes mechanically unstable because $\partial\Pi/\partial h > 0$, and the liquid flows away from the thin film. However, condensation would cause an increase in the film thickness for $h > h_C$. The transition from h_C to h_D is due to both the fluid flow and condensation. Therefore, the film thickness remains in the region $h_C < h < h_D$. We hypothesized that the film thickness is close to h_D. We note that the condensation was slow.

The contact line motion of evaporating drops, containing functionalized microspheres, was studied by Nguyen and Stebe.[41] Using fluorescence imaging, they observed coffee-ring formation and an abrupt change in the velocity during depinning of the contact line as a drop evaporated. They correlated these observations to Marangoni stress and convection caused by surfactant. Our experimental results

(41) Nguyen, V. X.; Stebe, K. J. *Phys. Rev. Lett.* **2002**, *88*, 164501.

explain the details of the contact line motion and the effect of surfactant adsorption as a drop evaporated or condensed.

F. Comparison of the Contact Line Motion and Shape Evolution with a Drop of a Pure Fluid. The process of surfactant-laden drop evolution can be compared with that for a pure fluid. Our earlier studies[7,9] for a pure fluid showed that during evaporation and condensation the apparent contact angle of the drop remained constant and that the velocity of the contact line was also constant. The drop shape evolved in a self-similar manner symmetrically and uniformly on all sides during evaporation or condensation. However, as is shown in Figures 12 and 16, because of the presence of the surfactant, the apparent contact angle for the drop changed as the contact line receded or advanced. The position of the point of inflection of the slope-angle profile of the drop also changed as the drop shape evolved. The contact line velocity for the surfactant-laden drop underwent abrupt changes during the shape evolution, as is shown in Figures 18 and 19. Hence, for the case of the drop of the surfactant, the shape evolves in a non-self-similar manner. Thus, the presence of the surfactant affects the contact line motion of the drop. This was explained in the previous section on the basis of the adsorption of the trisiloxane surfactant and its ability to form aggregates in the solution.

IV. Conclusions

An image analysis technique based on the reflectivity measurement of a thin film was used to experimentally study the advance and recession of the contact line of a surfactant-laden drop during evaporation and condensation. The drop solution was a water−surfactant (polyalkyleneoxide-modified heptamethyltrisiloxane, called a superspreader) mixture on a fused silica surface. We found that under isothermal conditions the surfactant formed a stable adsorbed film on the surface with a thickness of 31 nm. The stability of the film was analyzed using the concept of minimization of the interfacial free energy. During evaporative phase change, the adsorbed film breaks into microdrops, which are surrounded by a different, stable, thin adsorbed film. Whether evaporation or condensation is occurring, the thicknesses of these adsorbed films is lower than those under isothermal conditions.

We measured the complete interfacial profiles of surfactant-laden microdrops during evaporation and condensation. We found that the apparent contact angle of the drop increased during condensation and decreased during evaporation. The results were compared with that of the drop of a pure fluid, for which the apparent contact angle remained constant at a constant velocity during spreading and evaporation (self-similar shape evolution). We found that because of the presence of the surfactant the shape of the drop evolves in a non-self-similar shape manner (the contact line of the drop was pinned). When the surfactant film is just hydrated or desiccated during a phase change, there is an abrupt change in the drop velocity. This was explained on the basis of the adsorption of the trisiloxane surfactant at the interface and the ability of the surfactant to form aggregates in the solution. The experimental results give new insights into the effects of the trisiloxane surfactant on the shape evolution of a drop during phase-change phenomena.

Acknowledgment. This material is based on the work supported by the National Aeronautics and Space Administration under grant nos. NAG3-2383 and NNC05GA27G. Any opinions, findings, and conclusions or recommendations expressed in this publication are those of the authors and do not necessarily reflect the view of NASA.

LA050603U